Synthesis, Photophysics, Electrochemistry, and Reactivity of Ruthenium(II) Polypyridine Complexes with Organoplatinum(II) Moieties. Crystal Structure of $[Ru(bpy)_2(\mu\text{-}2,3\text{-dpp})PdCl_2]^{2+}$

Vivian Wing-Wah Yam,* Vicky Wing-Man Lee, and Kung-Kai Cheung

Department of Chemistry, The University of Hong Kong, Pokfulam Road, Hong Kong

Received December 17, 1996[⊗]

A series of luminescent ruthenium(II) polypyridine complexes with organoplatinum(II) moieties, together with their chloro precursors and palladium(II) dichloro analogues, $[Ru(bpy)_2(BL)MX_2]^{2+}$ (BL = 2,3-dpp, M = Pd, X = Cl (**1**); M = Pt, X = Cl (**2**), Cl and CH_3 (**3**), CH_3 (**4**), C_6H_5 (**5**), C_6H_4-OCH_3-*p* (**6**), C_6H_4-F-*p* (**7**); BL = bpm, M = Pd, X = Cl (**8**); M = Pt, X = Cl (**9**), Cl and CH_3 (**10**), C_6H_5 (**11**), C_6H_4-CH_3-*o* (**12**), C_6H_4-OCH_3-*p* (**13**), C_6H_4-F-*p* (**14**); BL = 2,3-dpq, M = Pt, R = C_6H_4-OCH_3-*p* (**15**)) have been synthesized and their electrochemical and photophysical properties studied; their reactivities toward the oxidative addition of methyl iodide have been investigated. The X-ray crystal structure of **1** has been determined.

The synthesis and design of supramolecular systems capable of performing photoinduced energy migration and/or charge separation have attracted current interest and efforts.[1] Ruthenium(II) complexes of polypyridine-type ligands have been widely used as building blocks for synthesizing redox-active and luminescent supramolecular metal complexes.[1−23] Related studies on organometallic complexes are rare,[3] in particular, the non-carbonyl-containing organometallics.[4] In our recent communication,[5] we showed that introduction of chloro and organo functions would serve to reduce the overall positive charge of the polynuclear complexes and, in the latter case, to increase the hydrophobicity of the complexes and render them more soluble in common organic solvents. In addition, organometallic components incorporated into the supramolecule, with the influence of other tunable building blocks, are expected to exhibit reactivity patterns quite different from their mononuclear counterparts, making this class of complexes more attractive to study. As an extension of our recent work, we report the synthesis, characterization, photophysics, and electrochemistry of two series of ruthenium(II) polypyridines with organoplatinum(II) moieties, together with their dichloro precursors and dichloropalladium analogue, using bridging ligands such as bpm (2,2′-bipyrimidine) and 2,3-dpp (2,3-bis(2-pyridyl)pyrazine). Studies on the reaction kinetics of the oxidative addition reaction, which is commonly observed in a variety of monomeric platinum(II) complexes, of these heterobimetallic complexes with alkyl halides are also described. The details of the crystal structure determination of $[Ru(bpy)_2(\mu\text{-}2,3\text{-dpp})PdCl_2]^{2+}$, which was previously communicated,[5] will also be described.

Experimental Section

Ruthenium trichloride was obtained from Johnson-Matthey Chemical Company. 2,2′-Bipyridine (bpy), 2,2′-bipyrimidine (bpm), and 2,3-bis(2-pyridyl)pyrazine (2,3-dpp) were obtained from the Aldrich Chemical Co. Dichloro(1,5-cyclooctadiene)-platinum(II) and potassium tetrachloroplatinate(II) were purchased from Strem Chemicals Inc. 2,3-Bis(2′-pyridyl)quinoxaline (2,3-dpq),[6] precursor complexes with bridging ligand BL, $[Ru(bpy)_2(BL)]^{2+}$,[3] $Pd(DMSO)_2Cl_2$, $Pt(DMSO)_2Cl_2$,[7] $Pt(DMSO)_2$-

[⊗] Abstract published in *Advance ACS Abstracts,* May 15, 1997.

(1) Balzani, V.; Scandola, F. *Supramolecular Photochemistry*; Horwood: Chichester, England, 1990.
(2) See, for example: (a) Denti, G.; Serroni, S.; Campagna, S.; Ricevuto, V.; Balzani, V. *Coord. Chem. Rev.* **1991**, *111*, 227. (b) Scanola, F.; Indelli, M. T.; Chiorboli, C.; Bignozzi, C. A. *Top. Curr. Chem.* **1990**, *158*, 73. (c) Balzani, V.; Juris, A.; Venturi, M.; Campagna, S.; Serroni, S. *Chem. Rev.* **1996**, *96*, 759 and references therein.
(3) Denti, G.; Campagna, S.; Sabatino, L.; Serroni, S.; Ciano, M.; Balzani, V. *Inorg. Chem.* **1990**, *29*, 4750.
(4) See, for example: (a) Scott, J. D.; Puddephatt, R. J. *Organometallics* **1986**, *5*, 2522. (b) Lanza, S. *Inorg. Chim. Acta* **1983**, *75*, 131. (c) Sutcliffe, V. F.; Young, G. B. *Polyhedron* **1984**, *3*, 87. (d) Braterman, P. S.; Song, J. I.; Volger, C.; Kaim, W. *Inorg. Chem.* **1992**, *31*, 222. (e) Chassot, L.; von Zelewsky, A.; Sandrini, D.; Maestri, M.; Balzani, V. *J. Am. Chem. Soc.* **1986**, *108*, 6084.
(5) Yam, V. W. W.; Lee, V. W. M.; Cheung, K. K. *J. Chem. Soc., Chem. Commun.* **1994**, 2075.
(6) Goodwin, H. A.; Lions, F. *J. Am. Chem. Soc.* **1959**, *81*, 6415.
(7) Price, J. H.; Williamson, A. N.; Schramm, R. F.; Wayland, B. B. *Inorg. Chem.* **1972**, *11*, 1284.
(8) Eaboron, C.; Kundu, K.; Pidcock, A. *J. Chem. Soc., Dalton Trans.* **1981**, 933.
(9) Cornioley-Deuschel, C.; von Zelewsky, A. *Inorg. Chem.* **1987**, *26*, 3354.
(10) Clark, H. C.; Manzer, L. E. *J. Organomet, Chem.* **1973**, *59*, 411.
(11) (a) Sahai, R.; Rillema, D. P. *Inorg. Chim. Acta* **1986**, *118*, L35. (b) Sahai, R.; Baucom, D. A.; Rillema, D. P. *Inorg. Chem.* **1986**, *25*, 3843.
(12) Braunstein, C. H.; Baker, A. D.; Strekas, T. C.; Gafney, H. D. *Inorg. Chem.* **1984**, *23*, 857.
(13) Sahai, R.; Rillema, D. P.; Shaver, R.; Wallendael, S. V.; Jackman, D. C.; Boldaji, M. *Inorg. Chem.* **1989**, *28*, 1022.
(14) Milkevitch, M.; Brauns, E.; Brewer, K. J. *Inorg. Chem.* **1996**, *35*, 1737.
(15) Roffia, S.; Marcaccio, M.; Paradisi, C.; Paolucci, F.; Balzani, V.; Denti, G.; Serroni, S.; Campagna, S. *Inorg. Chem.* **1993**, *32*, 3003.
(16) Chan, C. W.; Cheng, L. K.; Che, C. M. *Coord. Chem. Rev.* **1994**, *132*, 87.
(17) Scott, J. D.; Puddephatt, R. J. *Organometallics* **1986**, *5*, 1538.
(18) Kalyanasundaram, K.; Nazeeruddin, Md. K. *Inorg. Chem.* **1990**, *29*, 1888.
(19) Crespo, M.; Puddephatt, R. J. *Organometallics* **1987**, *6*, 2548.
(20) Green, M. L. H. *Organometallic Compounds*; Methnen: London, 1968; Vol. 2.
(21) Jawad, J. K.; Puddephatt, R. J. *J. Chem. Soc., Dalton Trans.* **1977**, 1466.
(22) Monaghan, P. K.; Puddephatt, R. J. *J. Chem. Soc., Dalton Trans.* **1988**, 595.
(23) Monaghan, P. K.; Puddephatt, R. J. *Inorg. Chim. Acta* **1983**, *76*, L237.

S0276-7333(96)01058-8 CCC: $14.00

(Cl)(CH_3), Pt(DMSO)$_2$(CH_3)$_2$,[8] Pt(Et_2S)$_2R_2$,[9] and Pt(cod)R_2[10] were prepared according to literature procedures. All other reagents were of analytical grade and were used as received.

Synthesis of Ruthenium(II)−Platinum(II) Complexes. [Ru(bpy)$_2$(μ-2,3-dpp)PdCl$_2$](PF$_6$)$_2$ (1). A mixture of [Ru(bpy)$_2$(2,3-dpp)](OTf)$_2$ (95 mg, 0.10 mmol) and Pd(DMSO)$_2$Cl$_2$ (50 mg, 0.15 mmol) was refluxed in ethanol (20 mL) for 24 h. The resulting dark purple solution was then filtered and concentrated. A dark purple solid was isolated by addition of NH_4PF_6. Diffusion of diethyl ether into an acetonitrile or acetone solution of the complex gave shiny dark purple cubic crystals. Yield: 89 mg, 80%. ^{1}H NMR (300 MHz, CD_3CN, 298 K, relative to Me_4Si): δ 7.3−9.2 (m, 26H, aromatic H). Anal. Calcd for $C_{34}H_{26}N_8P_2F_{12}RuPdCl_2$·$(CH_3)_2CO$: C, 37.9; H, 2.8; N, 9.5; Cl, 6.0. Found: C, 37.6; H, 2.5; N, 9.8; Cl, 5.8.

[Ru(bpy)$_2$(μ-2,3-dpp)PtCl$_2$](PF$_6$)$_2$ (2). The procedure was similar to that for **1** except Pt(DMSO)$_2$Cl$_2$ (60 mg, 0.15 mmol) was used instead of [Pd(DMSO)$_2$Cl$_2$] to give purplish red cubic crystals of **2**. Yield: 96 mg, 80%. ^{1}H NMR (300 MHz, CD_3CN, 298 K, relative to Me_4Si): δ 7.3−9.6 (m, 26H, aromatic H). Anal. Calcd for $C_{34}H_{26}N_8P_2F_{12}RuPtCl_2$: C, 33.9; H, 2.2; N, 9.3; Cl, 5.9. Found: C, 34.1; H, 2.3; N, 9.2; Cl, 6.0.

[Ru(bpy)$_2$(μ-2,3-dpp)PtCl(CH$_3$)](PF$_6$)$_2$ (3). A mixture of [Ru(bpy)$_2$(2,3-dpp)](PF$_6$)$_2$ (95 mg, 0.10 mmol) and [Pt(DMSO)$_2$Cl(CH_3)] (50 mg, 0.13 mmol) was stirred under nitrogen in acetone (15 ml) at room temperature for 2 h. The resulting dark purple solution was then filtered and concentrated. Slow diffusion of diethyl ether into an acetone or dichloromethane solution of the complex gave dark crystals of **3**. Yield: 95 mg, 80%. ^{1}H NMR (300 MHz, acetone-d_6, 298 K, relative to Me_4Si): δ 1.05, 1.30 (s, 3H, CH_3, J(Pt−H) = 87 Hz), 7.20−9.40 (m, 26H, aromatic H). Positive FAB-MS: ion clusters at m/z 895 {M}$^+$, 880 {M − CH_3}$^+$. Anal. Calcd for $C_{35}H_{29}N_8ClP_2F_{12}RuPt$·$^1/_2CH_2Cl_2$: C, 34.79; H, 2.47; N, 9.14. Found: C, 34.92; H, 2.39; N, 8.94.

[Ru(bpy)$_2$(μ-2,3-dpp)Pt(CH$_3$)$_2$](PF$_6$)$_2$ (4). The procedure was similar to that of **3** except Pt(DMSO)$_2$(CH_3)$_2$ (57 mg, 0.15 mmol) was used instead of [Pt(DMSO)$_2$Cl(CH_3)] to give dark purplish crystals of **4**. Yield: 76 mg, 65%. ^{1}H NMR (270 MHz, acetone-d_6, 298 K, relative to Me_4Si): δ 1.01 (s, 3H, CH_3, J(Pt−H) = 87 Hz), 1.43 (s, 3H, CH_3, J(Pt−H) = 88 Hz), 7.5−9.4 (m, 26H, aromatic H). Positive FAB-MS: m/z at 874 {M + 2}$^+$, 857 {M − CH_3}$^+$, 842 {M − 2CH_3}$^+$, 647 {M − Pt(CH_3)$_2$}$^+$. Anal. Calcd for $C_{36}H_{32}N_8P_2F_{12}RuPt$·$1.5CH_2Cl_2$: C, 34.9; H, 2.7; N, 8.7. Found: C, 35.0; H, 2.9; N, 8.6.

[Ru(bpy)$_2$(μ-2,3-dpp)Pt(C$_6$H$_5$)$_2$](PF$_6$)$_2$ (5). A mixture of [Ru(bpy)$_2$(2,3-dpp)](PF$_6$)$_2$ (95 mg, 0.1 mmol) and [Pt(cod)(C_6H_5)$_2$] (69 mg, 0.15 mmol) was refluxed in acetonitrile (15 mL) for 24 h. The resulting dark purple solution was then filtered and concentrated. Slow diffusion of diethyl ether into an acetonitrile solution of the complex gave dark brown crystals of **5**. Yield: 77 mg, 60%. ^{1}H NMR (300 MHz, acetone-d_6, 298 K, relative to Me_4Si): δ 7.50−9.40 (m, 36H, aromatic H). Positive FAB-MS: ion clusters at m/z 999 {M}$^+$, 922 {M − C_6H_5}$^+$, 845 {M − 2C_6H_5}$^+$. Anal. Calcd for $C_{46}H_{36}N_8P_2F_{12}RuPt$·$2H_2O$: C, 41.76; H, 3.05; N, 8.47. Found: C, 41.73; H, 2.78; N, 8.55.

[Ru(bpy)$_2$(μ-2,3-dpp)Pt(C$_6$H$_4$-OCH$_3$-*p*)$_2$](PF$_6$)$_2$ (6). The procedure was similar to that for **5** except [Pt(cod)(C_6H_4-OCH_3-*p*)$_2$] (78 mg, 0.15 mmol) was used instead of [Pt(cod)(C_6H_5)$_2$] to give dark red crystals of **6**. Yield: 104 mg, 77%. ^{1}H NMR (300 MHz, CD_3CN, 298 K, relative to Me_4Si): δ 3.65 (s, 3H, OCH_3), 3.70 (s, 3H, OCH_3), 6.62−6.69 (m, 4H, aromatic H), 7.10−8.70 (m, 30H, aromatic H). Positive FAB-MS: ion clusters at m/z 1202 {M·PF$_6$}$^+$, 1056 {M}$^+$, 948 {M − (C_6H_4-OCH_3-*p*)}$^+$, 841 {M − 2(C_6H_4-OCH_3-*p*)}$^+$. Anal. Calcd for $C_{48}H_{40}N_8O_2P_2F_{12}RuPt$: C, 42.80; H, 2.99; N 8.32. Found: C, 43.50; H, 2.96; N 8.55.

[Ru(bpy)$_2$(μ-2,3-dpp)Pt(C$_6$H$_4$-F-*p*)$_2$](PF$_6$)$_2$ (7). The procedure was similar to that for **5** except [Pt(cod)(C_6H_4-F-*p*)$_2$] (74 mg, 0.15 mmol) was used instead of [Pt(cod)(C_6H_5)$_2$] to give reddish brown crystals of **7**. Yield: 86 mg, 65%. ^{1}H NMR (300 MHz, CD_3CN, 298 K): δ 6.70−6.90 (m, 4H, aromatic H), 7.15−8.20 (m, 22H, aromatic H), 8.30−8.65 (m, 8H, aromatic H). Positive FAB-MS: ion clusters at m/z 1177 {M·PF$_6$}$^+$, 1032 {M}$^+$, 937 {M − (C_6H_4-F-*p*)}$^+$. Anal. Calcd for $C_{46}H_{34}N_8P_2F_{14}RuPt$: C, 41.76; H, 2.59; N, 8.47. Found: C, 41.68; H, 2.83; N, 8.42.

[Ru(bpy)$_2$(μ-bpm)PdCl$_2$](ClO$_4$)$_2$ (8). The procedure was similar to that for **1** except [Ru(bpy)$_2$(bpm)](ClO$_4$)$_2$ was used in place of [Ru(bpy)$_2$(2,3-dpp)](OTf)$_2$. Diffusion of diethyl ether into an acetonitrile solution of the complex gave shiny dark green cubic crystals of **8**. Yield: 71 mg, 75%. ^{1}H NMR (300 MHz, CD_3CN, 298 K, relative to Me_4Si): δ 7.40 (m, 4H, bpy), 7.50 (t, J = 5.7 Hz, 2H, bpm), 7.70 (m, 2H, bpy), 7.90 (d, J = 5.6 Hz, 2H, bpy), 8.05 (d, J = 6.3 Hz, 2H, bpm), 8.10 (m, 4H, bpy), 8.50 (d, J = 8.6 Hz, 4H, bpy), 9.10 (d, J = 6.3 Hz, 2H, bpm). Positive FAB-MS: ion clusters at m/z 851 {M·ClO$_4$}$^+$, 752 {M}$^+$. Anal. Calcd for $C_{28}H_{22}N_8O_8Cl_4RuPd$: C, 35.48; H, 2.34; N, 11.82. Found: C, 35.00; H, 2.34; N, 11.75.

[Ru(bpy)$_2$(μ-bpm)PtCl$_2$](PF$_6$)$_2$ (9). The procedure was similar to that reported by Rillema and co-workers.[11] Diffusion of diethyl ether into an acetonitrile solution of the complex gave shiny dark green cubic crystals. Yield: 85 mg, 75%. ^{1}H NMR (270 MHz, CD_3CN, 298 K): δ 7.43 (t, J = 5.7 Hz, 2H, bpy), 7.53 (t, J = 5.7 Hz, 2H, bpy), 7.64 (d, J = 5.7 Hz, 2H, bpy), 7.80 (t, J = 5.8 Hz, 2H, bpm), 8.05 (d, J = 5.8 Hz, 2H, bpy), 8.15 (m, 4H, bpy), 8.30 (d, J = 5.8 Hz, 2H, bpm), 8.50 (d, J = 5.7 Hz, 4H, bpy), 9.69 (d, J = 5.8 Hz, 2H, bpm). Positive FAB-MS: ion clusters at m/z 984 {M·PF$_6$}$^+$, 839 {M}$^+$.

[Ru(bpy)$_2$(μ-bpm)PtCl(CH$_3$)](ClO$_4$)$_2$ (10). The procedure was similar to that for **3** except [Ru(bpy)$_2$(bpm)](ClO$_4$)$_2$ (77 mg, 0.1 mmol) was used instead of [Ru(bpy)$_2$(2,3-dpp)](PF$_6$)$_2$ to give violet crystals of **10**. Yield: 80 mg, 79%. ^{1}H NMR (300 MHz, CD_3CN, 298 K, relative to Me_4Si): δ 1.27 (s, J(Pt−H) = 82 Hz, 3H, PtCH_3), 7.40−7.54 (m, 4H, bpy), 7.68 (t, J = 5.6 Hz, 1H, bpm), 7.86 (t, J = 5.6 Hz, 1H, bpm), 7.97−8.02 (m, 6H, bpy), 8.05 (d, J = 5.7 Hz, 2H, bpy), 8.29 (d, J = 5.6 Hz, 1H, bpm), 8.34 (d, J = 5.6 Hz, 1H, bpm), 8.51 (d, J = 8.2 Hz, 4H, bpy), 9.38 (d, J = 5.6 Hz, 1H, bpm), 9.56 (d, J = 5.6 Hz, 1H, bpm). Positive FAB-MS: ion clusters at m/z 917 {M·ClO$_4$}$^+$, 817 {M}$^+$, 802 {M − CH_3}$^+$. Anal. Calcd for $C_{29}H_{25}N_8O_8Cl_3RuPt$·$2.5CH_2Cl_2$: C, 32.54; H, 2.85; N, 10.56. Found: C, 32.45; H, 2.80; N, 10.56.

[Ru(bpy)$_2$(μ-bpm)Pt(C$_6$H$_5$)$_2$](PF$_6$)$_2$ (11). The procedure was similar to that for **5** except [Ru(bpy)$_2$(bpm)](PF$_6$)$_2$ (86 mg, 0.1 mmol) was used instead of [Ru(bpy)$_2$(2,3-dpp)](PF$_6$)$_2$ to give brownish red crystals of **11**. Yield: 81 mg, 67%. ^{1}H NMR (300 MHz, CD_3CN, 298 K, relative to Me_4Si): δ 6.89 (t, J = 7.2 Hz, 2H, H_{para}), 7.01 (t, J = 7.3 Hz, 4H, H_{meta}), 7.35 (d, J = 7.5 Hz, 4H, H_{ortho}), 7.42 (t, J = 7.4 Hz, 2H, bpy), 7.53 (t, J = 7.4 Hz, 2H, bpy), 7.60 (t, J = 5.6 Hz, 2H, bpm), 7.66 (d, J = 5.7 Hz, 2H, bpy), 8.03 (d, J = 5.6 Hz, 2H, bpy), 8.10 (t, J = 8.2 Hz, 2H, bpy), 8.15 (t, J = 8.2 Hz, 2H, bpy), 8.26 (d, J = 5.4 Hz, 2H, bpm), 8.51 (d, J = 8.2 Hz, 4H, bpy), 8.67 (d, J = 5.4 Hz, 2H, bpm). Anal. Calcd for $C_{40}H_{32}N_8P_2F_{12}RuPt$: C, 39.68; H, 2.66; N, 9.25. Found: C, 39.87; H, 2.87; N, 9.11.

[Ru(bpy)$_2$(μ-bpm)Pt(C$_6$H$_4$-CH$_3$-*o*)$_2$](PF$_6$)$_2$ (12). The procedure was similar to that for **11** except [Pt(cod)(C_6H_4-CH_3-*o*)$_2$] (73 mg, 0.15 mmol) was used instead of [Pt(cod)(C_6H_5)$_2$] to give dark red crystals of **12**. Yield: 84 mg, 68%. ^{1}H NMR (300 MHz, CD_3CN, 298 K, relative to Me_4Si): δ 2.65 (s, J(Pt−H) = 25 Hz, 6H, CH_3), 6.70−7.20 (m, 6H, H_{meta} and H_{para}), 7.30 (d, J = 7.0 Hz, 2H, H_{ortho}), 7.42 (t, J = 5.6 Hz, 2H, bpy), 7.53 (t, J = 5.6 Hz, 2H, bpy), 7.58 (t, J = 5.6 Hz, 2H, bpm), 7.67 (d, J = 5.6 Hz, 2H, bpy), 8.03 (d, J = 5.6 Hz, 2H, bpy), 8.10 (t, J = 8.1 Hz, 2H, bpy), 8.15 (t, J = 8.1 Hz, 2H, bpy), 8.30 (d, J = 5.6 Hz, 2H, bpm), 8.51 (d, J = 8.2 Hz, 4H, bpy), 8.70 (d, J = 5.6 Hz, 2H, bpm). Positive FAB-MS: ion clusters at m/z 1095 {M·PF$_6$}$^+$, 952 {M}$^+$. Anal. Calcd for $C_{42}H_{36}N_8P_2F_{12}RuPt$·$CH_2Cl_2$·$CH_3CN$: C, 39.57; H, 3.00; N, 9.23. Found: C, 39.62; H, 2.68; N, 9.63.

[Ru(bpy)$_2$(μ-bpm)Pt(C$_6$H$_4$-OCH$_3$-*p*)$_2$](PF$_6$)$_2$ (13). The procedure was similar to that for **11** except [Pt(cod)(C_6H_4-OCH_3-

p)$_2$] (78 mg, 0.15 mmol) was used instead of [Pt(cod)(C$_6$H$_5$)$_2$] to give dark red crystals of **13**. Yield: 83 mg, 65%. ^{1}H NMR (300 MHz, CD$_3$CN, 298 K, relative to Me$_4$Si): δ 3.70 (s, 6H, OCH$_3$), 6.69 (d, J = 6.9 Hz, 4H, H$_{meta}$), 7.20 (d, J = 6.9 Hz, 4H, H$_{ortho}$), 7.42 (t, J = 5.6 Hz, 2H, bpy), 7.53 (t, J = 5.6 Hz, 2H, bpy), 7.60 (t, J = 5.6 Hz, 2H, bpm), 7.67 (d, J = 5.6 Hz, 2H, bpy), 8.03 (d, J = 5.6 Hz, 2H, bpy), 8.10 (t, J = 8.2 Hz, 2H, bpy), 8.15 (t, J = 8.2 Hz, 2H, bpy), 8.27 (d, J = 5.7 Hz, 2H, bpm), 8.51 (d, J = 8.2 Hz, 4H, bpy), 8.72 (d, J = 5.6 Hz, 2H, bpm). Positive FAB-MS: ion clusters at m/z 1127 {M·PF$_6$}$^+$, 980 {M}$^+$, 491 {M}$^{2+}$. Anal. Calcd for C$_{42}$H$_{36}$N$_8$O$_2$P$_2$F$_{12}$RuPt·H$_2$O: C, 39.14; H, 2.97; N, 8.69. Found: C, 38.90; H, 2.87; N, 8.87.

[Ru(bpy)$_2$(μ-bpm)Pt(C$_6$H$_4$-F-*p*)$_2$](PF$_6$)$_2$ (14). The procedure was similar to that for **11** except [Pt(cod)(C$_6$H$_4$-F-*p*)$_2$] (74 mg, 0.15 mmol) was used instead of [Pt(cod)(C$_6$H$_5$)$_2$] to give dark red crystals of **14**. Yield: 85 mg, 68%. ^{1}H NMR (300 MHz, CD$_3$CN, 298 K, relative to Me$_4$Si): δ 6.82−6.86 (m, 4H, H$_{meta}$), 7.29−7.32 (m, 4H, H$_{ortho}$), 7.43 (d, J = 5.4 Hz, 2H, bpy), 7.55 (t, J = 7.4 Hz, 2H, bpy), 7.60 (t, J = 5.5 Hz, 2H, bpm), 7.68 (d, J = 5.7 Hz, 2H, bpy), 8.05 (d, J = 5.7 Hz, 2H, bpy), 8.10 (t, J = 7.4 Hz, 2H, bpy), 8.15 (t, J = 7.4 Hz, 2H, bpy), 8.25 (d, J = 5.5 Hz, 2H, bpm), 8.51 (d, J = 8.2 Hz, 4H, bpy), 8.62 (d, J = 5.5 Hz, 2H, bpm). Positive FAB-MS: ion clusters at m/z 1103 {M·PF$_6$}$^+$. Anal. Calcd for C$_{40}$H$_{30}$N$_8$P$_2$F$_{14}$RuPt: C, 38.53; H, 2.43; N, 8.99. Found: C, 38.22; H, 2.65; N, 8.97.

[Ru(bpy)$_2$(μ-2,3-dpq)Pt(C$_6$H$_4$-OCH$_3$-*p*)$_2$](ClO$_4$)$_2$ (15). A mixture of [Ru(bpy)$_2$(2,3-dpq)](ClO$_4$)$_2$ (134 mg, 0.1 mmol) and [Pt(C$_6$H$_4$-OCH$_3$-*p*)$_2$]$_2$(μ-Et$_2$S)$_2$ (70 mg, 0.07 mmol) was stirred in 15 mL of acetone under an inert atmosphere for 24 h. The resultant dark purple solution was filtered, and the diffusion of diethyl ether into the filtrate afforded dark purple crystals of **15**. Yield: 106 mg, 81%. ^{1}H NMR (300 MHz, CD$_3$CN, 298 K, relative to Me$_4$Si): δ 3.64 (s, 3H, OCH$_3$), 3.66 (s, 3H, OCH$_3$), 6.5 (m, 4H, aromatic H), 6.95 (m, 4H, aromatic H), 7.25−7.75 (m, 12H, aromatic H), 7.80−8.30 (m, 12H, aromatic H), 8.65−8.75 (m, 4H, aromatic H). Positive FAB-MS: ion clusters at m/z 1203 {M·ClO$_4$}$^+$. Anal. Calcd for C$_{52}$H$_{42}$N$_8$O$_2$P$_2$F$_{12}$RuPt·2.5H$_2$O: C, 43.3; H, 3.28; N, 7.77. Found: C, 43.05; H, 3.03; N, 8.09.

Physical Measurements and Instrumentation. UV/visible spectra were obtained on a Hewlett-Packard 8452A diode array spectrophotometer, and steady-state excitation and emission spectra on a Spex Fluorolog 111 spectrofluorometer. Low-temperature (77 K) spectra were recorded by using an optical Dewar sample holder. ^{1}H NMR spectra were recorded on a Bruker DPX-300 Fourier transform NMR spectrometer with chemical shifts reported relative to tetramethylsilane. Positive ion FAB mass spectra were recorded on a Finnigan MAT95 mass spectrometer. Elemental analyses of the new complexes were performed by Butterworth Laboratories Ltd.

Emission lifetime measurements were performed using a conventional laser system. The excitation source was the 355-nm output (third harmonic) of a Quanta-Ray Q-switched GCR-150-10 pulsed Nd-YAG laser (pulse width 8 ns). Luminescence decay signals were recorded on a Tektronix Model TDS 620A digital oscilloscope and analyzed using a program for exponential fits. All solutions for photophysical studies were prepared under vacuum in a 10-cm^3 round-bottomed flask equipped with a side-arm 1-cm fluorescence cuvette and sealed from the atmosphere with a Kontes quick-release Teflon stopper. Solutions were rigorously degassed with no fewer than four freeze−pump−thaw cycles (final pressure < 10^{-5} Torr).

Cyclic voltammetric measurements were carried out with a PAR model 175 universal programmer and Model 173 potentiostat. Cyclic voltammograms were recorded with a Kipp & Zonen BD90 $X-Y$ recorder at scan rates of 50−500 mV s^{-1}. The electrolytic cell used was a conventional two compartment cell. The reference electrode is the Ag/AgNO$_3$ (0.1 M in acetonitrile) electrode with a Vycor glass interfacing the working electrode compartment. Electrochemical studies were performed in nonaqueous medium (0.1 M NBu$_4$PF$_6$ in acetonitrile) with the glassy carbon (Atomergic Chemetal V25) electrode as working electrode and a piece of platinum gauze as counter electrode which is separated from the working electrode by a sintered glass frit. The ferrocenium/ferrocene couple (FeCp$_2^{+/0}$) was used as the internal reference in nonaqueous media.

Kinetic studies of the reactions between Ru−Pt organometallic complexes and methyl iodide were carried out in acetonitrile solution using an excess of methyl iodide and monitoring the decay of the MLCT absorption band of the complex at 550−600 nm. Stock solutions of the heterobimetallic ruthenium(II)−platinum(II) complexes in the required solvent were prepared. An exact volume of the stock solution was transferred to a 1-cm quartz UV cell held in the sample chamber of a HP-8452A spectrophotometer and allowed to equilibrate for 15 min to the required temperature which is in the range 15−50 °C maintained by a Lauda R6M compact thermostat. A known amount of methyl iodide was added to the solution in the UV cell with a 25-μL Hamilton microsyringe and mixed thoroughly. The initial concentration of the heterobimetallic complex was always in the order of 10^{-4} mol dm^{-3}.

Crystal Structure Determination. [Ru(bpy)$_2$(μ-2,3-dpp)PdCl$_2$]$^{2+}$ (1). Crystal Data. [C$_{34}$H$_{26}$N$_8$Cl$_2$PdRu]$^{2+}$·2(PF$_6$)$^-$, M = 1114.94, monoclinic, space group $P2_1/c$, a = 12.413(4) Å, b = 23.758(6) Å, c = 14.863(3) Å, β = 93.25(2)°, V = 4376.4(1.0) Å^3, Z = 4, D_c = 1.693 g cm^{-3}, μ(Mo Kα) = 10.24 cm^{-1}, F(000) = 2192, T = 297 K. A crystal of dimensions 0.10 × 0.15 × 0.35 mm was used for the measurement of diffraction data made on an Enraf-Nonius CAD-4 diffractometer with graphite-monochromatized Mo Kα radiation (λ = 0.710 73 Å) using $\omega-2\theta$ scans with ω-scan angle (1.20 + 0.344 tan θ)° at a scan speed of 2.06−5.49° min^{-1}. Intensity data (in the range of $2\theta_{max}$ = 47°, h, 0 −13; k, 0−26; l, −16 to 16, and three standard reflections measured every 2 h showed no decay) were corrected for Lorentz and polarization effects and empirical absorption corrections based on the ψ-scan of five strong reflections (minimum and maximum transmission factors 0.946 and 0.998, respectively). Upon averaging the 6997 reflections, 6311 of which measured once, 6654 independent reflections were obtained (R_{int} = 0.06 for all the 340 reflections measured twice), 3218 reflections with $I \geq 3.0\sigma(I)$ were considered observed and used in the structural analysis. The space group was determined from systematic absences and the solution of the structure by Patterson and Fourier methods and subsequent refinement by full-matrix least squares using the Enraf-Nonius SDP-1985 programs on a MicroVax II computer. All the 60 non-hydrogen atoms were refined anisotropically, and the 26 H atoms at calculated positions with isotropic thermal parameters equal to 1.3 times that of the attached C atom were not refined. Convergence for 541 variable parameters by least-squares refinement on F with $w = 4F_o^2/\sigma^2(F_o^2)$, where $\sigma^2(F_o^2) = [\sigma^2(I) + (0.055F_o^2)^2]$ for reflections with $I \geq 3.0\sigma(I)$, were reached at R = 0.076 and wR = 0.098 with a goodness of fit of 2.117 for 3218 reflections with $I \geq 3.0\sigma(I)$. $(\Delta/\sigma)_{max}$ = 0.02. A final difference Fourier map was featureless, with maximum positive and negative peaks of 1.62 and 0.94 e Å^{-3}, respectively. The crystal and structure determination data are collected in Table 1. Complete bond distances and angles, atomic coordinates, and thermal parameters have been included in the Supporting Information.

Results and Discussion

The ruthenium(II)−platinum(II) heterobimetallic complexes were prepared by the reaction of the corresponding dialkyl- or diarylplatinum(II) precursor with [Ru(bpy)$_2$(BL)]$^{2+}$. Other related ruthenium(II) supramolecules have been prepared using a similar synthetic strategy.[11] All the newly synthesized complexes gave satisfactory elemental analyses and have been characterized by positive FAB-MS and ^{1}H NMR spectroscopy.

Table 1. Crystal and Structure Determination data for 1

formula	$[C_{34}H_{26}N_8Cl_2PdRu]^{2+}\cdot 2(PF_6)^-$
M_r	1114.94
T, K	297
a, Å	12.413(4)
b, Å	23.758(6)
c, Å	14.863(3)
β, deg	93.25(2)
V, Å^3	4376.4(1.0)
crystal color and shape	dark green shiny block
crystal system	monoclinic
space group	$P2_1/c$
Z	4
$F(000)$	2192
D_c, g cm^{-3}	1.693
crystal dimensions, mm	0.10 × 0.15 × 0.35
λ, Å (graphite monochromated, Mo Kα)	0.710 73
μ, cm^{-1}	10.24
collection range	$2\theta_{max} = 47°$ (h, 0 to 13; k, 0 to 26; l, −16 to 16)
scan mode and scan speed, deg min^{-1}	$\omega-2\theta$; 2.06 to 5.49
scan width, deg	1.20 + 0.344 tan θ
no. of data collected	6997
no of unique data	6654
no. of data used in refinement, m	3218
no. of parameters refined, p	541
R^a	0.076
$R_w{}^a$	0.098
goodness of fit, S	2.117
maximum shift, $(\Delta/\sigma)_{max}$	0.02
residual extrema in final difference map, e Å^{-3}	+1.62, −0.94

[a] $w = 4F_o^2/\sigma^2(F_o^2)$, where $\sigma^2(F_o^2) = [\sigma^2(I) + (0.055\ F_o^2)^2]$ with $I > 3.0\sigma(I)$.

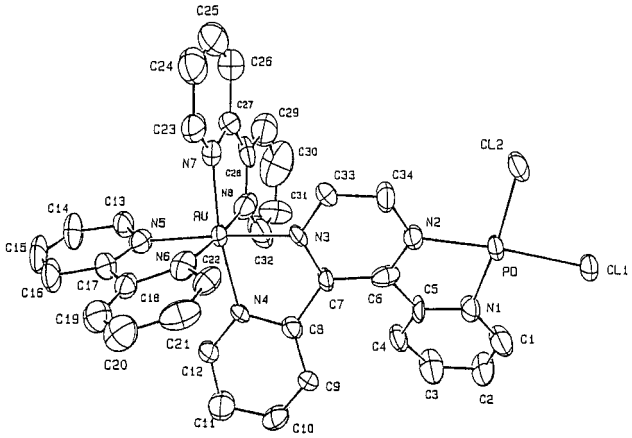

Figure 1. Perspective drawing of **1** with the atomic numbering scheme.

Complexes **1** and **2** have also been characterized crystallographically, and the crystal struture of **2** has been described previously.[5]

Figure 1 depicts the perspective drawing of **1** with the atomic numbering scheme. The selected bond lengths and bond angles of **1** are collected in Table 2. The complex is isostructural to **2** with the Ru atom in a distorted octahedral geometry and the Pd atom being slightly distorted square-planar. All bond distances and angles in **2** reported previously and those of **1** are normal and are very similar. The N−Ru−N bond angles subtended by the chelating diimines are in the range of 78.4(5)−80.3(6)°, much distorted from a regular octahedral geometry as a result of the steric requirement of the diimines. It is interesting to note that the pyridine and pyrazine rings of the 2,3-dpp ligand are not coplanar. Unlike the mononuclear $[Ru(bpy)_2(2,3\text{-dpp})]^{2+}$, where one pyridine ring of 2,3-dpp is orthogonal to the plane of the other pyridine and pyrazine rings, both pyridine rings are forced toward planarity with the pyrazine ring in the formation of the binuclear complexes.[12] This causes significant steric crowding between the hydrogens on the pyridine rings, leading to planes containing the coordinating nitrogens and the metal ion tilted relative to each other. In **1**, the pyridine ring containing N(1) attached to the Pd atom is tilted 21.5(1.0)° relative to the pyrazine ring and 43.8(7)° relative to the other pyridine ring of 2,3-dpp containing N(4) attached to Ru. A tilting angle of as much as 35−40° relative to each other has been estimated from molecular modeling studies.[12] The two pyridine rings of the bipyridine ligand containing N(7) and N(8) in **1** are least distorted from coplanarity, indicating least steric overcrowding experienced in that plane. Similar findings have also been observed in complex **2**.[5]

The electrochemical data for the heterobimetallic complexes are summarized in Table 3. The cyclic voltammograms of $[Ru(bpy)_2(BL)PtR_2]^{2+}$ show irreversible oxidation waves and a quasi-reversible oxidation couple ($\Delta E_p \approx 70$ mV) and three to four reversible reduction couples ($\Delta E_p \approx 60$ mV). The nature of the irreversible oxidation processes is tentatively assigned as the platinum(II)-based oxidation that generates an unstable platinum(III) species. The quasi-reversible oxidation couple is assigned as a one-electron ruthenium-based oxidation. The reduction waves were assigned to reduction processes as given in the following scheme:

$$[Ru^{II}(bpy)_2(BL)PtR_2]^{2+} + e^- \rightleftharpoons [Ru^{II}(bpy)_2(BL^{\bullet-})PtR_2]^+$$

$$[Ru^{II}(bpy)_2(BL^{\bullet-})PtR_2]^+ + e^- \rightleftharpoons [Ru^{II}(bpy)_2(BL^{2-})PtR_2]^0$$

$$[Ru^{II}(bpy)_2(BL^{2-})PtR_2]^0 + e^- \rightleftharpoons [Ru^{II}(bpy)(bpy^{\bullet-})(BL^{2-})PtR_2]^-$$

$$[Ru^{II}(bpy)(bpy^{\bullet-})(BL^{2-})PtR_2]^- + e^- \rightleftharpoons [Ru^{II}(bpy^{\bullet-})_2(BL^{2-})PtR_2]^{2-}$$

In all the bimetallic complexes, the first two reduction waves are assigned to the successive one-electron reduction of the bridging 2,3-dpp or bpm ligand. The two subsequent reductions have been assigned to the sequential one-electron reduction on each of the bpy ligands coordinated to the ruthenium(II) center. Similar assignments have been reported for other homo-[3] and heterobimetallic[11,13,14] complexes of ruthenium(II).

The BL-based reduction potentials in the heterobimetallic complexes were shifted to more positive values relative to the corresponding $[Ru(bpy)_2(BL)]^{2+}$ complex, in accord with the increased ease of the bridging ligand-based reduction upon coordination of a second metal ion.[3,15] The ease of BL-based reduction for $[Ru(bpy)_2(\mu\text{-bpm})PtR_2]^{2+}$ follows the order **12** < **13** ≈ **11** < **14**, while that for $[Ru(bpy)_2(\mu\text{-2,3-dpp})PtR_2]^{2+}$ is in the order **2** > **3** > **4** and $[Ru(bpy)(\mu\text{-2,3-dpp})PtAr_2]^{2+}$ > **4**. The observed trend is in line with the donating ability of

Table 2. Selected Bond Lengths and Angles (with Estimated Standard Deviations in Parentheses) for 1

Bond Lengths, Å			
Pd−Cl(1)	2.283(5)	Ru−N(4)	2.03(1)
Pd−Cl(2)	2.280(6)	Ru−N(5)	2.07(2)
Pd−N(1)	2.00(1)	Ru−N(6)	2.04(2)
Pd−N(2)	2.03(1)	Ru−N(7)	2.03(1)
Ru−N(3)	2.03(1)	Ru−N(8)	2.00(2)
Angles, deg			
Cl(1)−Pd−Cl(2)	91.1(2)	N(1)−Pd−N(2)	79.6(6)
Cl(1)−Pd−N(1)	94.3(4)	N(3)−Ru−N(4)	78.4(5)
Cl(1)−Pd−N(2)	174.2(4)	N(5)−Ru−N(6)	79.9(6)
Cl(2)−Pd−N(1)	173.2(5)	N(7)−Ru−N(8)	80.3(6)
Cl(2)−Pd−N(2)	94.7(4)		

Dihedral Angles, deg	
N(1)C(1)C(2)C(3)C(4)C(5)−N(2)C(6)C(7)N(3)C(33)C(34)	21.5(1.0)
N(1)C(1)C(2)C(3)C(4)C(5)−N(4)C(8)C(9)C(10)C(11)C(12)	43.8(7)
N(2)C(6)C(7)N(3)C(33)C(4)−N(4)C(8)C(9)C(10)C(11)C(12)	27.3(9)

Table 3. Electrochemical Data for Complexes 1−14[a]

complex	oxidation $E_{1/2}$ (E_{pa}), V *vs* SCE	reduction $E_{1/2}$(E_{pc}), V *vs* SCE
1	+1.56	(−0.54, −0.79), −1.08, −1.51, −1.76
2	(+1.47), +1.57	−0.54, −1.11, −1.49
3	+1.58	−0.65, −1.23, −1.51, −1.73
4	(+0.66, +1.12), +1.63	−0.84, −1.39, −1.61, −1.83
5	+1.62	−0.76, −1.28, −1.53, −1.74
6	(+1.67), +1.76	−0.76, −1.30, −1.52, −1.73
7	(+1.30), +1.61	−0.74, −1.27, −1.52, −1.72
8	(+1.57), +1.61	−0.32, −1.03, −1.47, −1.71
9	(+1.60), +1.70	−0.30, −1.02, −1.52, −1.75
10	+1.74	−0.49, −1.22, −1.60, −1.85
11	(+1.23), +1.72	−0.56, −1.26, −1.58, −1.82
12	(+1.33), +1.39	−0.57, −1.27, −1.58, −1.83
13	(+0.96, +1.27), +1.40	−0.56, −1.26, −1.58, −1.82
14	(+1.34), +1.73	−0.53, −1.24, −1.58, −1.82

[a] In acetonitrile solution containing 0.1 mol dm^{-3} NBu_4PF_6 as supporting electrolyte.

the alkyl and aryl groups. The most electron-withdrawing C_6H_4-F-*p* moiety would render the ligand-centered reduction easiest and the ruthenium-centered oxidation most difficult. Similarly, replacement of the electronegative chloro ligand by the more electron-rich methyl group on the platinum(II) center would enhance the back π-bonding to μ-BL. On the other hand, the aryl substituents, which are less electron-rich σ-donors than the alkyls and also are π-acceptors, would render the platinum(II) less electron-rich, leading to a comparatively weaker back π-bonding interaction with the bridging ligand and a less negative ligand-centered reduction potential is expected.

The electronic absorption spectral data of the complexes are tabulated in Table 4. The electronic absorption spectra of the complexes are dominated by intense absorption bands of ligand-based π−π* and n−π* transitions in the UV region and MLCT transitions in the visible region. The intense high energy band at ∼282 nm is assigned as bpy-centered π−π* transition while the shoulder at ∼310 nm probably arises from the π−π* transition of the bridging bpm ligand for the complexes bridged by bpm, and the absorption at ∼330 nm corresponds to that of the bridging μ-2,3-dpp ligand for those bridged by 2,3-dpp.

The low-energy absorptions in the visible region consist of overlapping bands of ^{1}MLCT transitions, dominated by [dπ(Ru) → π*(bpy)] and [dπ(Ru) → π*(BL)] with some contribution from [d(Pt) → π*(BL)]. Rilemma and co-workers also assigned a 324-nm absorption band ($\epsilon = 1.8 \times 10^4$ dm^3 mol^{-1} cm^{-1}) in a related heterometallic Ru−Pt complex as [d(Pt) → π*(Mebpy−Mebpy)] MLCT transition.[11b] With the much lower-lying π* energy of 2,3-dpp and bpm relative to Mebpy−Mebpy and the more electron-rich Pt center, in particular those with σ-donating alkyl and aryl groups attached to it, the [d(Pt) → π*(2,3-dpp) or π*(bpm)] MLCT transition would be expected to occur at low energies with $\lambda > 324$ nm. A low-energy [d(Pt) → π*(phen)] MLCT transition band with extinction coefficient of the order of 10^3 dm^3 mol^{-1} cm^{-1} has also been reported to occur at ∼400 nm in a monomeric [Pt(phen)(C≡CPh)$_2$] complex.[16] Low-energy absorption bands at ∼482 ($\epsilon = 1960$ dm^3 mol^{-1} cm^{-1}), 504 ($\epsilon = 3290$ dm^3 mol^{-1} cm^{-1}), and 538 nm ($\epsilon = 9730$ dm^3 mol^{-1} cm^{-1}) have been observed in the related [PtMe$_2$(bpm)], [PtMe$_2$(2,3-dpp)], and [Me$_2$Pt(μ-2,3-dpp)PtMe$_2$], respectively, as the respective [d(Pt) → π*(bpm)],[4a,17] [d(Pt) → π*(2,3-dpp)],[4a] and [d(Pt) → π*(μ-2,3-dpp)][4a] MLCT transition. The higher energy MLCT transition at ∼414−416 nm in [Ru(bpy)$_2$(μ-bpm)PtR$_2$]$^{2+}$ and ∼422−430 nm in [Ru(bpy)$_2$(μ-2,3-dpp)PtR$_2$]$^{2+}$ are assigned as the dπ(Ru) → π*(bpy) transition. Corresponding transitions were observed at ∼422 and ∼434 nm for the monomeric [Ru(bpy)$_2$(bpm)]$^{2+}$ and [Ru(bpy)$_2$(2,3-dpp)]$^{2+}$,[18] respectively, where, upon incorporation of the PtR$_2$ moieties, a blue shift in the transition energy is observed relative to that of the monomer. Similar shifts have been reported in the homobimetallic [{Ru(bpy)$_2$}$_2$(μ-bpm)]$^{4+}$ and [{Ru(bpy)$_2$}$_2$(μ-2,3-dpp)]$^{4+}$.[18] This is understandable as introduction of a second metal fragment could be considered as attaching an electron-withdrawing substituent on the bridging ligand, resulting in the lowering of the π*-energy level of the bridging ligand, as well as causing a slight lowering of the dπ energy level of Ru(II), leading to a blue shift in the dπ(Ru) → π*(bpy) MLCT transition energy, and a red shift in the dπ(Ru) → π*(BL) MLCT transition band, which occurs at lower energy. This is in agreement with the increased ease of reduction of the bridging ligand in the electrochemical studies, indicating the lowering of the π*(BL) energy level upon coordination of a second metal center to the bridging ligand.

The mononuclear complex [Ru(bpy)$_2$(BL)]$^{2+}$ is strongly emissive both in fluid solutions and in the solid state at room temperature. Upon coordination of the second metal center, the luminescent properties were altered with a general trend of shifting the emission wavelength to the red and causing an attenuation in the emission quantum yield. Excitation of fluid solutions of the heterobimetallic complexes at $\lambda > 350$ nm at room temperature or the EtOH/MeOH (v/v 4:1) glass at 77 K resulted in red emission, typical of ^{3}MLCT emission. All of them are only weakly emissive to nonemissive in the solid state. The photophysical data are summarized in Table 4.

The emission spectra of complexes **2**−**4** and [Ru(bpy)$_2$(2,3-dpp)]$^{2+}$ in acetonitrile at room temperature are depicted in Figure 2. The emission is derived from the lowest lying triplet MLCT [dπ(Ru) → π*(2,3-dpp)] with energies in the order [Ru(bpy)$_2$(2,3-dpp)]$^{2+}$ > **4** > **3** > **2**. The observed trend is in good agreement with the

Table 4. Electronic Absorption Spectral and Photophysical Data for 1−14

complex	λ_{abs}/nm (ϵ, mol^{-1} dm^3 cm^{-1})	medium (T, K)	emission max, nm	τ_o, μs
1	284 (55 200), 425 (19 800), 526 (24 800)	CH_3CN (298)	700	0.37
		glass[a] (77)	700	4.00
2	422 (9290), 509 (15 200)	CH_3CN (298)	800	0.45
		glass[a] (77)	752	2.20
3	286 (49 000), 430 (9540), 498 (14 000)	CH_3CN (298)	778	0.30
		glass[a] (77)	717	2.00
4	437 (13 100), 524 (12 000)	Me_2CO (298)	735	0.33
5	286 (63 100), 430 (12 700), 484 (14 600), 514 (13 900)	CH_3CN (298)	703	0.30
		glass[a] (77)	675	2.40
6	286 (32 900), 430 (6700), 496 (8250), 610 (sh) (2070)	CH_3CN (298)	686	0.39
		glass[a] (77)	680	1.90
7	286 (44 200), 430 (9170), 480 (10 900), 511 (11 300)	CH_3CN (298)	698	0.43
		glass[a] (77)	673	2.60
8	282 (51 900), 414 (14 400), 556 (2560)		*b*	
9	280 (51 200), 414 (16 300), 568 (3670)		*b*	
10	282 (47 600), 410 (14 300), 556 (4580), 592 (2430)	CH_3CN (298)	813	0.09
11	284 (40 300), 410 (18 700), 528 (5850), 568 (5310)	CH_3CN (298)	697	0.09
		glass[a] (77)	706	0.14
12	284 (60 300). 414 (18 900), 490 (6170), 556 (3240)	CH_3CN (298)	716	0.09
		glass[a] (77)	635	0.77
13	284 (66 300), 416 (19 900), 490 (6530), 554 (3330)	CH_3CN (298)	713	0.09
		glass[a] (77)	637	0.73
14	282 (61 700), 410 (20 100), 540 (6180)	CH_3CN (298)	700	0.09
		glass[a] (77)	706	0.18

[a] Electronic absorption measurement was made in acetonitrile at 298 K; the emission of glass was taken in EtOH/MeOH (4:1 v/v) at 77 K. [b] Emission not detected up to 850 nm.

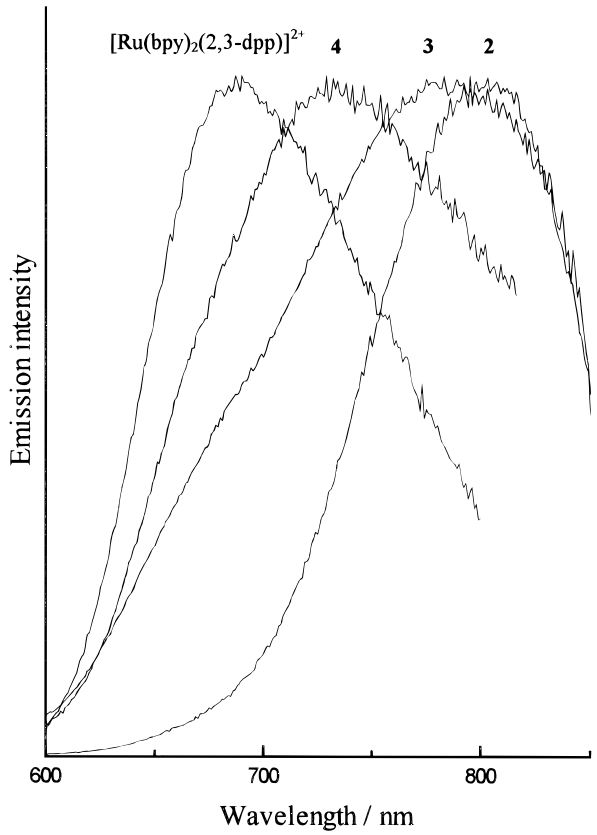

Figure 2. Normalized emission spectra of complexes **2**−**4** and $[Ru(bpy)_2(2,3\text{-dpp})]^{2+}$ in acetonitrile at 298 K with excitation wavelength at 350 nm.

ordering of the π^*(2,3-dpp) energies: 2,3-dpp > (μ-2,3-dpp)$Pt(CH_3)_2$ > (μ-2,3-dpp)$PtCl(CH_3)$ > (μ-2,3-dpp)$PtCl_2$. Similarly, the $[Ru(bpy)_2(\mu\text{-bpm})PtR_2]^{2+}$ complexes show emission energies in an order governed by the nature of the R group, with the emission energy lowest for the most electron-deficient $PtCl(CH_3)$ moieties in **10**. Thus, the emission of **10** at ~813 nm, which is at lower energy than that of $[Ru(bpy)_2(bpm)]^{2+}$ and complexes with diarylplatinum(II) components, is in line with the introduction of the platinum(II) fragment, which would lower the π^*-energy level of bpm and result in a lower $d\pi$(Ru) → π^*(bpm) ^{3}MLCT emission energy, while electron-donating aryl groups would render the platinum(II) center on PtR_2 more electron-rich relative to the $PtCl(CH_3)$ moiety and resulted in a higher π^*-energy level for bpm.

The complexes are stable in a variety of solvents such as dichloromethane, acetone, and acetonitrile. However, thermal reactions between $[Ru(bpy)_2(BL)PtR_2]^{2+}$ and alkyl halides such as methyl iodide have been observed at ambient conditions. It is speculated that the reaction is basically an oxidative addition of the alkyl halide to the dialkyl- or diarylplatinum(II) moiety. Similar observations have also been reported in a variety of monomeric platinum(II) complexes.[17,19] The identity of the oxidative addition products was established by FAB-MS and ^{1}H NMR spectroscopy.

^{1}H NMR studies on the oxidative addition products of complexes **6** and **13** in CD_3CN were undertaken. In both cases, a Pt−methyl signal at δ 1.54 with a typical Pt(IV)−H coupling constant of ~70 Hz appeared after addition of methyl iodide. The appearance of this Pt(IV)−methyl signal with the correct integral ratio confirms the identity of the oxidative addition product. In the case of complex **13**, there should be only one signal for the OCH_3 group in the *trans*-addition product with structure a, while either structure bI or bII of the *cis*-addition would result in a splitting of the OCH_3 signal as a result of loss of chemical and magnetic equivalence of the OCH_3 groups of structure b upon *cis*-addition of methyl iodide. The observation of two well-separated singlets at δ 3.56 and 3.58 with an integral ratio of 1:1 for the OCH_3 group in the oxidative addition product of **13** suggests the formation of a *cis*-addition product. Similarly, the splitting of the OCH_3 signals into three singlets at δ 3.83, 3.79, and 3.78 with an integral ratio of about 2:1:1 for the product of **6** also suggest a *cis*- addition product while only two singlets

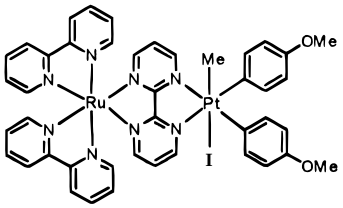

(a)

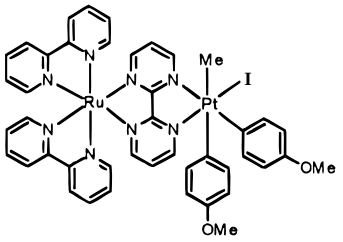

(bI)

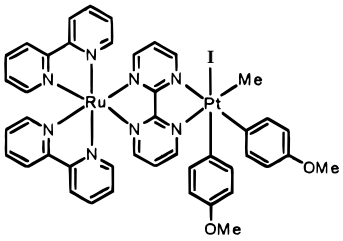

(bII)

with an integral ratio of 1:1 would be expected for the OCH_3 groups of the *trans*-addition product for **6**. In the mononuclear organoplatinum(II) complexes such as [Pt(L)R_2] where L is a diimine-type or phosphine type ligand, *trans*-addition products are usually obtained.[17,19]

Besides the change in ^{1}H NMR spectra, the electronic absorption spectra also undergo observable changes during the course of the reaction. Typical electronic absorption spectral traces during a kinetic run are shown in Figure 3. The reactions were found to be first order with respect to the complexes. Plots of observed pseudo-first-order rate constants (k_{obs}) vs the concentrations of methyl iodide for the various complexes gave satisfactory linear plots passing through the origin, revealing a first-order dependence of the reaction rate on the concentration of methyl iodide. The second-order rate constants, k_2, were determined from the slope of the plots in Figure 4 and are listed in Table 5.

The order of reactivities of the bpm bridged complexes with different R groups is reflected by the slopes of the plots: C_6H_4-OCH_3-*p* > C_6H_5 > C_6H_4-F-*p*. The results are consistent with the S_N2 mechanism suggested by previous studies on the oxidative addition reaction of alkyl halides with monomeric Pt(II) systems.[19] The C_6H_4-OCH_3-*p* group, being the most electron donating, renders the Pt(II) center most nucleophilic among the three complexes studied. Similarly, the second-order rate constant for **6** is larger than that of **7,** showing similar trends as the bpm series.

The high thermal stability of ortho-substituted aryl transition metal complexes compared with the para-substituted analogues has often been attributed to steric hindrance. The presence of ortho-substituent may prevent attack at the metal center by blocking the coordination sites above and below the square planar complexes.[20] Supportive evidence is provided by the observation that **12** does not react with methyl iodide, although **11** and **14** with comparatively less electron-

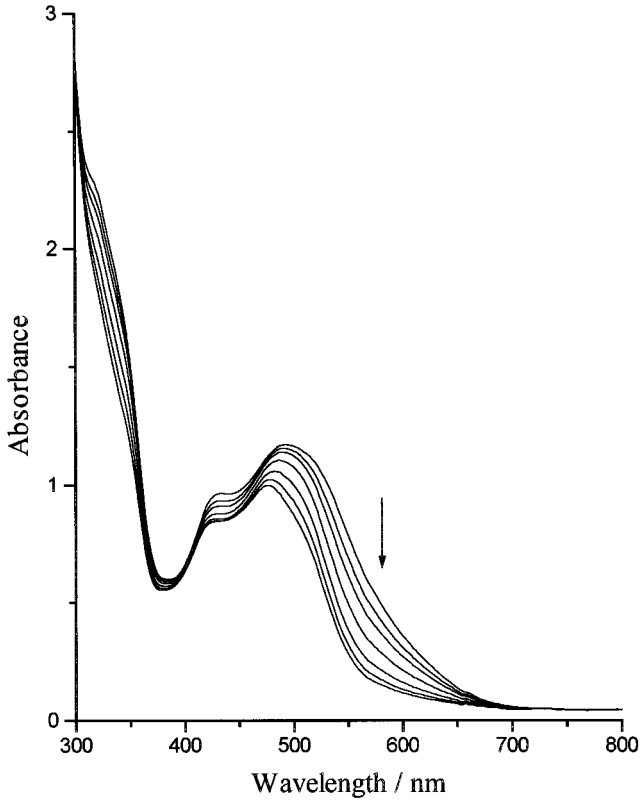

Figure 3. Electronic absorption spectral traces for the reaction between methyl iodide and **6** in acetonitrile at 298 K.

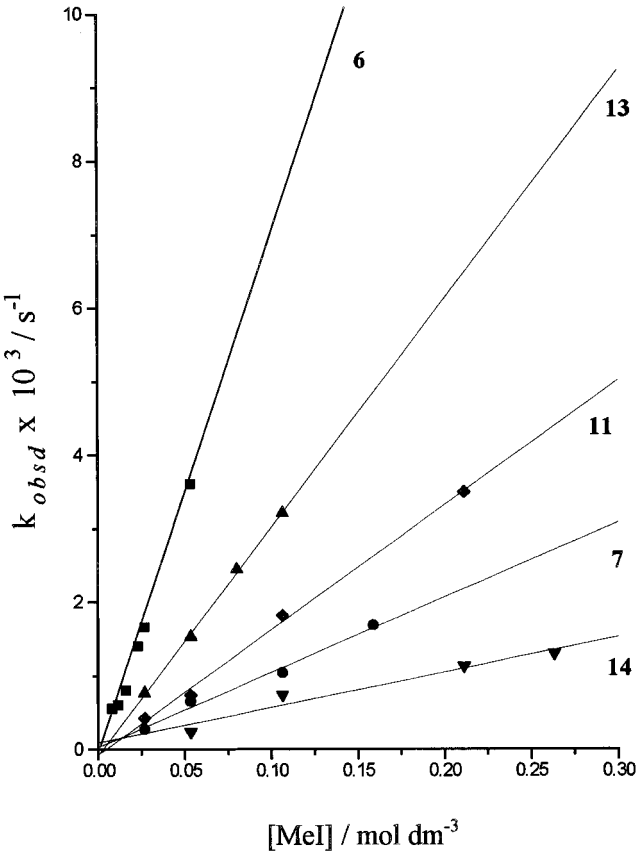

Figure 4. Pseudo-first-order reaction rate constants vs [MeI] in acetonitrile for complexes **6**, **7**, **11**, **13**, and **14** at 298 K.

Table 5. Second-Order Rate Constants for the Oxidative Addition of Methyl Iodide to Organometallic Heterometallic Complexes at 298 K and under 1 atm of Pressure

complex	second-order rate constant k_2, dm^3 mol^{-1} s^{-1}	solvent
6	6.96×10^{-2}	CH_3CN
	6.10×10^{-2}	CH_3CH_2CN
	3.46×10^{-2}	$(CH_3)_2CO$
	3.15×10^{-2}	CH_3OH
	7.28×10^{-3}	CH_2Cl_2
7	1.02×10^{-2}	CH_3CN
11	1.69×10^{-2}	CH_3CN
13	3.10×10^{-2}	CH_3CN
	2.37×10^{-2}	$(CH_3)_2CO$
14	4.77×10^{-2}	CH_3CN
15	6.47×10^{-2}	$(CH_3)_2CO$

rich Pt(II) center do react. The difference is presumably due to steric hindrance to the approach of methyl iodide to the platinum center in the ortho-substituted derivative.

The reaction rate constants for the reaction of methyl iodide and $[Ru(bpy)_2(BL)Pt(C_6H_4\text{-}OCH_3\text{-}p)_2]^{2+}$ with different bridging ligands, BL = bpm, 2,3-dpp, and 2,3-dpq, were investigated in acetone. The rate constants for complexes **6**, **13**, and **15** are of the order of 10^{-2} dm^3 mol^{-1} s^{-1}, while that reported for $[Pt(bpy)(C_6H_4\text{-}OCH_3\text{-}p)_2]$ is 82.5 dm^3 mol^{-1} s^{-1}.[21] The much smaller rate constants for the oxidative addition reaction of the heterobimetallic complexes $[Ru(bpy)_2(BL)Pt(C_6H_4\text{-}OCH_3\text{-}p)_2]^{2+}$ than for $[Pt(bpy)(C_6H_4\text{-}OCH_3\text{-}p)_2]$ are understandable as coordination of the electron-withdrawing Ru(bpy)$_2$ moiety would render the bridging ligand BL a weaker donor and therefore a lower reactivity in oxidative addition resulted. Moreover, the overall positive charge of 2+ in **6**, **13**, and **15** would also disfavor the oxidative addition reaction. The reactivity of the heterometallic complexes $[Ru(bpy)_2(BL)Pt(C_6H_4\text{-}OCH_3\text{-}p)_2]^{2+}$ follows the order **15** > **6** > **13**, which is not in line with the π^*-orbital energies of the bridging ligands, 2,3-dpp > bpm > 2,3-dpq, estimated from a knowledge of the first reduction potentials of $[Ru(bpy)_2(BL)]^{2+}$. The results were understandable in consideration that it is the $5d_{z^2}$ electron pair on platinum(II), which is involved in the nucleophilic attack in the oxidative addition reactions, the energy of which is expected to be governed by σ-bonding effects rather than the π-bonding effects.[4a]

The reactivity of the heterobimetallic complex with bridging bpm ligand is the lowest among the three complexes studied. Regarding the distance and the communication between the two metal centers, the analogues with bpm would be the one with the shortest distance and the best communication of the three candidates. Therefore, the effect of positively charged ruthenium fragment would be much more pronounced in bpm analogues compared to the other two. The ruthenium fragment could be viewed as an electron-withdrawing substituent that lowers the nucleophilicity of the platinum center, and as a result, the nucleophilic attack of platinum center to the alkyl halide would be slower.

Investigation of the effect of solvent on the oxidative addition of methyl iodide to **6** was carried out in five different solvents (Table 5). Similar electronic absorption spectral traces were obtained in all the solvents studied and the same oxidative addition product, $[Ru(bpy)_2(\mu\text{-}2,3\text{-}dpp)Pt^{IV}(C_6H_4\text{-}OCH_3\text{-}p)_2(CH_3)I]^{2+}$ was obtained, which was confirmed by positive FAB-MS data. The reaction rate in different solvents is in the order $CH_3CN > C_2H_5CN > (CH_3)_2CO \geq CH_3OH > CH_2Cl_2$, which is roughly in line with the polarity of the solvent, indicative by their dielectric constant values, which are in the order $CH_3CN > CH_3OH > C_2H_5CN > (CH_3)_2CO > CH_2Cl_2$. Except for the anomaly found in the case of methanol, the overall trend of the reaction rate shows a substantial dependence on the polarity of the solvent, with faster reactions in solvents of higher dielectric constants. Similar findings were obtained in the studies of the oxidative addition reaction of the monomeric platinum(II) counterparts $[Pt(bpy)_2R_2]$[21] and other related studies where a S_N2 mechanism is postulated.[4a]

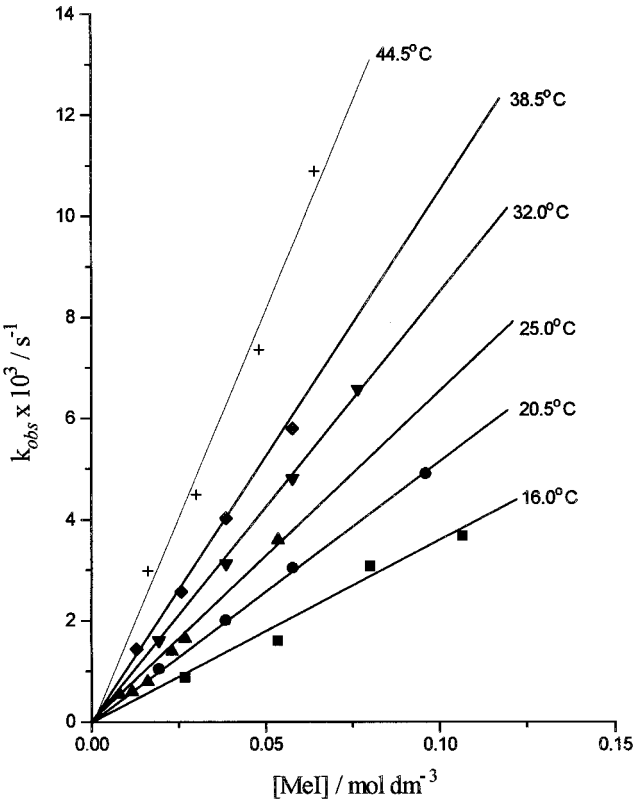

Figure 5. Pseudo-first-order reaction rate constants vs [MeI] at different temperatures for complex **6** in acetonitrile.

The temperature-dependence studies of the methyl iodide oxidative addition rate constants for complexes **6** and **7** have been determined at various temperatures ranging from 15 to 45 °C (Figure 5). The $\Delta S^{\ddagger}$ value is estimated to be −156 and −154 J K^{-1} mol^{-1}, respectively, for complexes **6** and **7** from the plot of $\ln(k_2/T)$ vs $1/T$ (Figure 6). A $\Delta H^{\ddagger}$ value of 33.3 and 37.9 kJ mol^{-1} has been obtained for complexes **6** and **7**, respectively. Similar results have been obtained in the related $[Pt(bpy)R_2]$ complexes.[21] The large negative value of $\Delta S^{\ddagger}$, typical of oxidative addition reactions, is suggestive of the involvement of an associative mechanism for the transition-state production in the rate-determining step. The close resemblance of the $\Delta S^{\ddagger}$ values of the complexes is suggestive of a similar pathway for the reactions.

Reactivity studies involving different alkyl halides have also been pursued. Similar electronic absorption spectral traces were obtained for the reaction with ethyl iodide. The k_2 value of 5×10^{-5} dm^3 mol^{-1} s^{-1} for the

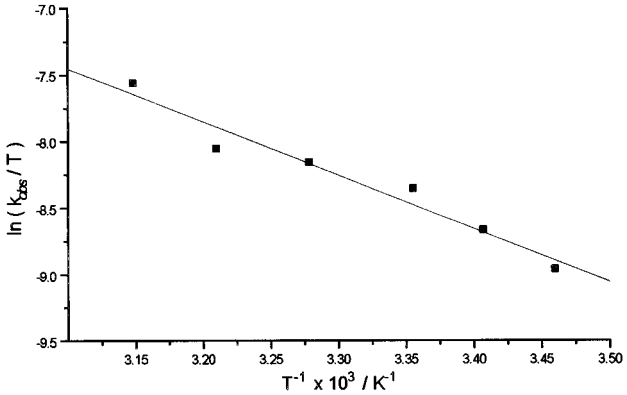

Figure 6. Eyring plot for the reaction of **6** and methyl iodide in acetonitrile.

reaction between **6** and ethyl iodide is much smaller than that with methyl iodide. Similar reactions with *n*-propyl iodide or *tert*-butyl iodide were too slow to be determined within a reasonable time scale. The observed trend is in line with that expected for an S_N2 mechanism and is consistent with our previous discussion. The lower reactivity of **6** toward ethyl iodide is understandable since the greater bulk of the ethyl group would probably introduce a greater hindrance to the nucleophilic attack of **6** on ethyl iodide. Similar observation in [Pt(CH$_3$)$_2$(phen)] has been reported in the literature,[22,23] where the oxidative addition rate constants for MeI/EtI/PrI/BuI were observed to be in the ratio of 1000:1:0.5:0.6.

The emission spectra of **6** recorded before and after the oxidative addition reaction with methyl iodide are depicted in Figure 7. With the excitation wavelength set at 380 nm, which is the isosbestic point of the electronic absorption traces under identical conditions, the solution emission of [Ru(bpy)$_2$(μ-2,3-dpp)Pt^{IV}(C$_6$H$_4$-OCH$_3$-*p*)$_2$(CH$_3$)I]$^{2+}$ is found to occur at lower energy and is at a higher intensity than its platinum(II) counterpart, **6**. It is likely that after oxidative addition, the organometallic Pt(IV) fragment becomes coordinately saturated, and as a result, nonradiative deactivation through exciplex quenching, which involves the interaction of the medium with the vacant site of the coordinate unsaturated square-planar organoplatinum(II), would be greatly diminished, giving rise to a higher luminescence quantum yield. The red shift that occurred upon oxidative addition of methyl iodide into the metal

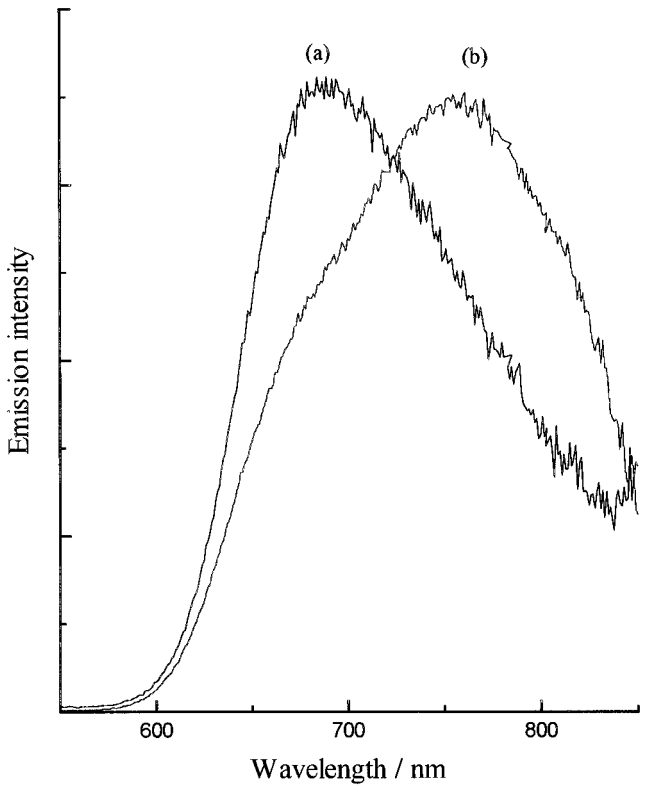

Figure 7. Emission spectra of **6** before addition of methyl iodide×14 (a) and after completion of oxidative addition reaction with methyl iodide (b).

complex may probably be a result of the more electron-deficient Pt(IV) center relative to the Pt(II), which would result in the lowering of the π*-energy level of the bridging ligand.

Acknowledgment. V.W.-W.Y. acknowledges financial support from the Research Grants Council and The University of Hong Kong. V.W.-M.L. acknowledges the receipt of a postgraduate studentship, administered by The University of Hong Kong.

Supporting Information Available: Tables of bond distances and angles, atomic coordinates, and thermal parameters for **1** (11 pages). Ordering information is given on any current masthead page.

OM961058I